Constraining the Neutron Star Equation of State with Observational Data

New Mexico
Supercomputing Challenge
Final Report
April 1, 2025

Los Alamos High School
Tate Plohr

Teacher:
JeeYeon Plohr

Mentors:
Ingo Tews, Rahul Somasundaram

EXECUTIVE SUMMARY

Neutron stars are remnants of the cores of massive stars after they undergo supernovae, powerful explosions, at the end of their lives. Neutron stars are so dense that electrons are forced into atomic nuclei, where they combine with protons to form neutrons. They were theoretically predicted in the 1930s and first observed in the 1960s. Since then, much research has been done to understand the properties of the neutron stars. In particular, the Equation of State for the neutron star is an active research area for its importance in astrophysics simulations as well as in condensed matter physics. In the last few years, unprecedented observational data from the Neutron star Interior Composition Explorer (NICER) and the Laser Interferometer Gravitational-wave Observatory (LIGO) on neutron stars became available, making it possible to test out numerous theories.

In nuclear physics, there are many proposed Equations of State (EOSs) for neutron stars based on theories with various assumptions and approximations. To find the true EOS for neutron stars, we adopted a data-oriented, model-agnostic approach, based on random sampling and Bayesian analysis. Starting with many possible EOSs, we utilized recent observational data of neutron stars to constrain these candidates. The prediction of the 90th percentile range of the radius of a 1.4-solar-mass neutron star provides a quantitative measure of the constraint and can be compared to other works.

One important question to be answered by research on the neutron star EOS is the composition of the core. That is, whether the cores of neutron stars are made of nucleonic matter, like the outer layers, or instead, it consists of quarks or exotic states of matter. Using the constrained set of EOSs, we investigated the state of matter at the core. By analyzing the structure of the likely EOS curves, I find the probability that the core is made of nucleons relative to the probability of deconfined quark matter. I find that nucleonic matter is strongly favored over deconfined quark matter. Specifically, nucleonic matter is 21 times more likely than quark matter.

Table of Contents

I. INTRODUCTION

1.1 Neutron Stars and Equation of State

All stars begin as stellar nebulae and are stabilized by nuclear fusion. Over millions or billions of years, they exhaust their fuel for fusion and can evolve into red giants or supergiants. The most massive stars undergo a supernova explosion, leaving behind a compact remnant. Lighter stars form white dwarfs, medium-mass stars evolve into neutron stars, and the most massive stars collapse into black holes. In this paper, I examine neutron stars, with a particular focus on their Equation of State (EOS), which is essential for understanding their properties.

Neutron stars are the densest observable objects in the universe, formed during the supernova explosions of red supergiant stars. A typical neutron star weighs about 1.4 times the mass of the Sun and has a radius between 10 and 12 km (Lattimer and Prakash, 2001), making the neutron star's core density exceed that of atomic nuclei. They are so dense that one sugar cube of neutron star matter would weigh 10 billion tons on Earth, or roughly 30,000 Empire State Buildings. However, we do not have reliable models of the extreme densities inside neutron stars. This is why studying neutron stars is crucial, since it allows physicists to create more refined models describing all matter at densities not currently achievable on Earth.

Neutron stars have several distinct layers: an atmosphere, outer crust, inner crust, outer core, and inner core (see Fig. 1). The atmosphere is a thin layer composed of hydrogen, helium, and carbon. Beneath it lies the solid outer crust, made up of ions and electrons arranged in a lattice structure. Below the outer crust is the inner crust, where nuclei are compressed so tightly that they can form “nuclear pasta” (Caplan and Horowitz, 2017). In the outer core, a neutron superfluid and a proton superconductor coexist. Finally, there is the inner core, where the composition is unknown due to the extremely high density. It may consist of neutrons and protons like the outer core, or it could be made of exotic matter, such as deconfined quark matter or (keep? ***) “hyperons,” which are subatomic particles that weigh more than protons and neutrons (Benhar, O. *et al.* (eds.), 2024).

Neutron stars provide an effective laboratory for studying matter and the laws of physics at extreme densities on the threshold of forming a black hole. Constraining the neutron star EOS improves our understanding of the interaction between the strong force and gravity.

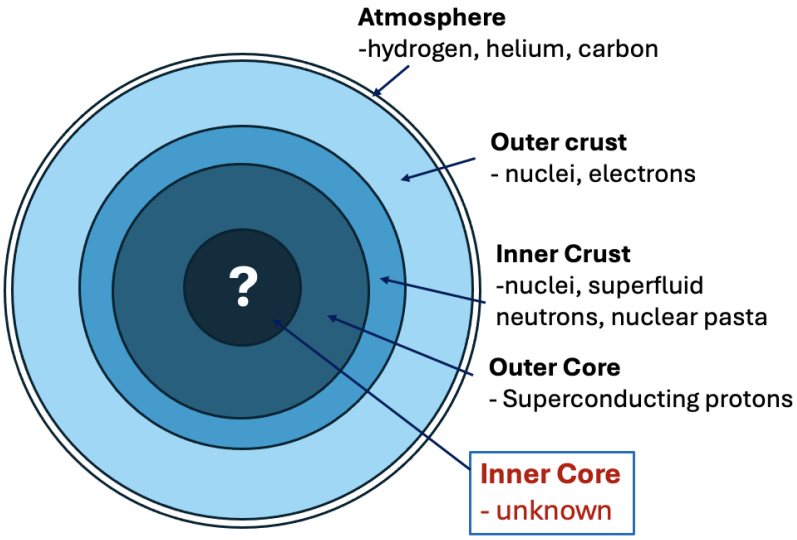

Figure 1: Inner structure of a neutron star.

The Equation of State (EOS) is a relationship between thermodynamic state variables such as density, pressure, temperature, energy, etc. For neutron star matter, we generally relate the pressure and the energy density or number density. At low densities, Chiral Effective Field Theory (Chiral EFT) provides a well-established description of the strong force between nucleons (neutrons and protons) (Epelbaum *et al.*, 2008). However, Chiral EFT breaks down at high densities. Beyond the breakdown density, many models have been proposed to describe the higher-density regime, each depending on different underlying physical assumptions and approximations. The uncertainty in this regime is represented by the blue region in Fig. 2. Even the precise value of the breakdown density remains uncertain (Capano *et al*., 2020). In this work, I assume the breakdown density to be 1.5 n_s, where n_s is the saturation density ($1.6 / fm^3$), the density of an atomic nucleus. This follows Dietrich *et al.,* 2020.

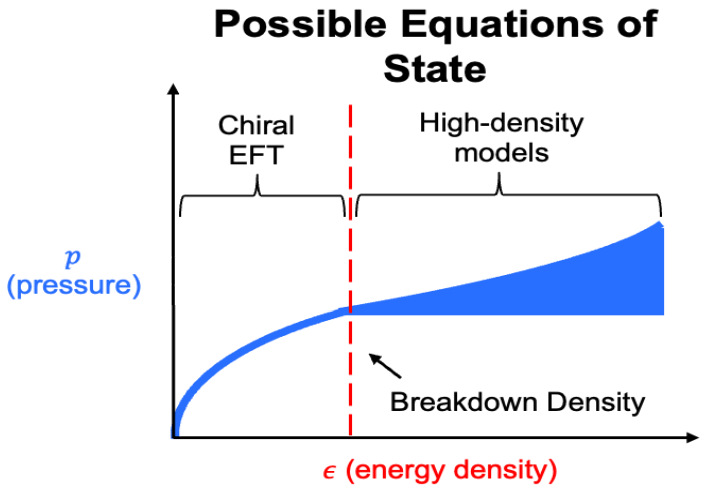

Figure 2: The Nuclear Matter Equation of State. The low-density regime is well constrained by theory. The regime beyond the breakdown density, however, is not well understood, and many possible EOSs have been proposed.

The purpose of this paper is to search for the unified EOS that describes all neutron stars. My approach involves generating 5,000 EOS samples that are constructed using Chiral EFT in the low-density regime and are random in the high-density regime (Tews, 2024). I use random samples to explore all possibilities in the high-density regime, to account for the numerous models that have been proposed. By adopting a model-agnostic approach, I allow the data to determine which EOSs are more probable. Following Dietrich et al., 2020, I construct an analysis framework with a Python program that converts the EOS curves into mass-radius curves, which are explained in the next section. Then, I combine the analysis of multiple neutron star datasets with existing nuclear theory to find the most probable EOSs using Bayesian statistical methods.

This framework is based on the hypothesis that, even though neutron stars have different sizes and masses, they all follow the one, true Neutron Star EOS. Therefore, every neutron star must fall somewhere on the one, true mass-radius curve. I am trying to find this mass-radius curve that predicts the mass-radius observations of several neutron stars. Once I calculate the probabilities of the EOS curves, I examine their predictions of neutron star properties. In particular, **the composition of the inner core, i.e., whether it is nucleonic (protons and neutrons) like the outer core or deconfined quark matter (QM), is encoded in the EOS curves.** To illustrate this point, let us consider water and vapor. When vapor condenses to water,

its density jumps with the sound speed increasing in proportion. This is manifested as a plateau in pressure vs. energy density. We can make analogous statements about nucleonic and deconfined quark matter. If the core consists of neutrons and protons, pressure will increase monotonically with energy. On the other hand, if the matter in the core has gone through a phase transition to become quark matter (QM), the pressure-energy curve will have a plateau. In other words, a change in the composition is likely manifested in the structure of EOS curves. Therefore, by analyzing the structure of the more probable EOS curves, I find out what the core is made of.

By reducing the uncertainty in the Equation of State, I identify which high-density models of particle physics are most accurate and best describe the properties of neutron stars. The EOS plays a crucial role in astrophysical simulations, so finding the true EOS helps us understand many phenomena of neutron stars. For example, when two neutron stars merge, new elements are created through what is known as the rapid process or r-process. A large fraction of natural elements heavier than iron are formed in such events, meaning that most objects in everyday life are made of elements from neutron stars. Physicists try to understand the r-process using computer simulations where the EOS is an essential component. Therefore, knowledge of the state of neutron stars is crucial in understanding how these elements were made and why some elements exhibit certain properties (Cowan *et al*. 2021).

1.2 Tolman-Oppenheimer-Volkoff Equations and Mass-Radius curves

To constrain the Neutron Star EOS with mass-radius data, I calculate the masses and radii of neutron stars predicted by each EOS by solving the Tolman-Oppenheimer-Volkoff (TOV) Equations, which describe a spherically symmetric object, such as a neutron star (Oppenheimer and Volkoff, 1939; Tolman, 1939; Camenzind, 2007; Gandolfi *et al.*, 2019). The details of a solver I wrote, using the forward Euler method in Python are in the appendix. These equations are based on the equilibrium between relativistic gravity and the pressure in nuclear matter. The TOV equations are Ordinary Differential Equations (ODEs):

$$\frac{dm}{dr} = 4\,\pi\, r^2\, \epsilon(P), \tag{1}$$

$$\frac{dP}{dr} = \frac{-G\, m(r)\, \epsilon(P)}{r^2\, c^2}\left(1 + \frac{4\,\pi\, r^3\, P}{m(r)\, c^2}\right)\left(1 + \frac{P}{\epsilon(P)}\right)\left(1 - \frac{2\, G\, m(r)}{r\, c^2}\right)^{-1}, \quad (2)$$

where $m(r)$ is the mass within the sphere of radius r; $P(r)$ is the pressure on the surface of that sphere; the total energy density $\epsilon(P)$ is specified by the EOS. The first factor corresponds to Newtonian gravity, the next three terms are relativistic corrections. To model a neutron star, I solve a boundary condition problem for the TOV equations with many choices of the central pressure P_c to find the total mass M and radius R of the neutron star. For each choice of P_c, I integrate the TOV equations with respect to r from $P = P_c$ and $m = 0$ at $r = 0$ until the pressure drops to zero, at which point $r = R$ and $m = M$. In this way, I obtain a curve relating the total mass M and radius R of the neutron star for a range of choices of the central pressure, which is the mass-radius curve for the EOS. A more detailed explanation of how to solve the TOV equations is in the Appendix.

In Fig. 3, I illustrate the result of integrating the TOV equations for an EOS to give its mass-radius curve. There is a one-to-one correspondence between the two curves so the probability of the mass-radius curve is equal to the probability of the corresponding EOS. In Fig. 4, I show my 5000 EOS samples and their corresponding mass-radius curves, obtained by my TOV solver.

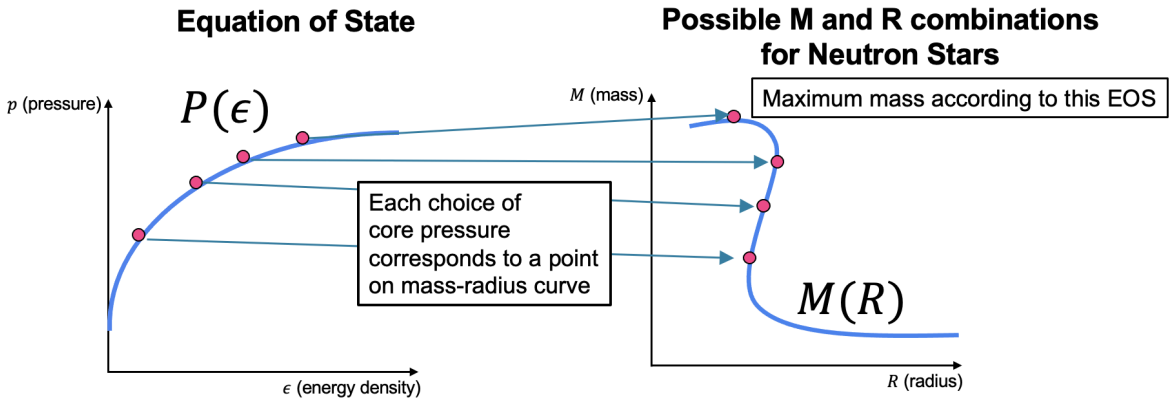

Figure 3: Integrating the TOV equations for each EOS results in a curve in the mass-radius plane.

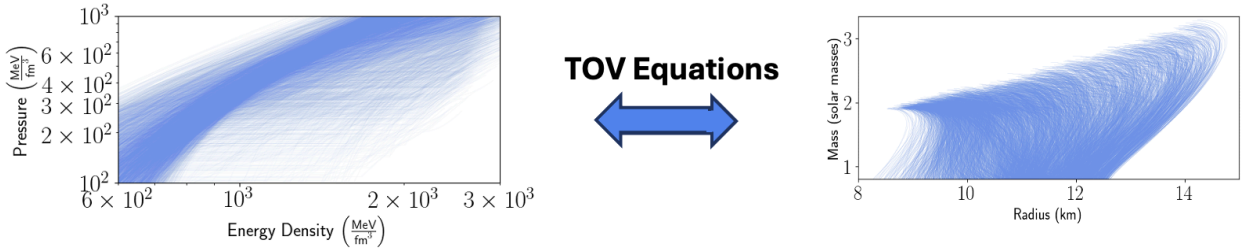

Figure 4: Neutron star mass-radius curves predicted by 5000 sample EOSs.

II. DATA

In this section, we review the three types of observational data on neutron stars that have been used in this work: data from radio observations, NICER X-ray observations, and LIGO gravitational-wave data. These public datasets are available in the form of tables. For instance, NICER data have thousands of pairs of mass and radius values. Collectively, they represent a probability distribution. The areas where there are more data points (of mass and radius) correspond to higher probabilities. I convert this table of discrete points into a probability distribution function using a Kernel Density Estimator or KDE, which is a standard statistical method. I utilized a KDE method in SciPy, a Python library. More details about the KDE can be found in the appendix.

2.1 *Maximum Mass Data*

The maximum mass data helps determine which mass-radius curve is more probable based on its prediction of the maximum mass of a neutron star. This data includes three pulsars that are contenders for the most massive neutron star observed (although we cannot be certain which one is the most massive due to measurement uncertainties). These massive pulsars provide a lower bound for how massive neutron stars can be (Rezzolla, *et al.*, 2018).

The data also includes a gravitational-wave event where two neutron stars collided, resulting in the lowest mass black hole we have observed. This black hole provides an upper bound on the maximum mass a neutron star can have (Abbott et al., 2017).

2.2 *NICER Data*

The Neutron Star Interior Composition Explorer (NICER) is an X-ray telescope onboard the International Space Station (ISS) that observes pulsars, rapidly rotating neutron stars. Pulsars have magnetic fields that emit X-rays from areas known as hotspots. NICER observes these

X-rays and obtains a “pulse profile.” These pulse profiles do not reveal much on their own, so researchers perform simulations of neutron stars with various parameters, including mass and radius. By comparing the resulting pulse profile from the simulation with the real pulse profile, mass and radius can be estimated. Among numerous neutron star observations, three analyses of neutron star pulse profiles are considered most credible and are utilized in this paper. For simplicity and clarity, I label these three NICER datasets in Table 1.

	NICER 1	NICER 2	NICER 3
Neutron star (pulsar)	PSR J0030+0451 (Miller *et al.,* 2019; Raaijmakers *et al.,* 2019)	PSR J0437-4715 (Choudhury *et al.*, 2024)	PSR J0740+6620 (Miller *et al.,* 2021; Riley *et al.*, 2021)

Table 1: Labels for the NICER data

I note that the PSR J0030+0451 pulse profiles have recently been reanalyzed using an updated framework (Vinciguerra *et al.*, 2024) that incorporates extra information. The new analysis yielded two modes in mass and radius, meaning two distinct pairs of mass and radius are likely. I identify which mode of mass and radius is more consistent with the observations of other neutron stars and present the result in an Appendix.

2.3 *LIGO/VIRGO Data*

The Laser Interferometer Gravitational-wave Observatory (LIGO) consists of two large observatories aimed at detecting gravitational waves using laser interferometry. VIRGO, named after a galaxy, is another such observatory in Europe. The collaboration between multiple detectors is crucial for gravitational wave measurement. Gravitational waves are released when two massive objects rapidly orbit each other and cause ripples in spacetime. These gravitational waves depend on the Chirp Mass (a combination of the masses of the two objects), the mass ratio between the objects, and the tidal deformability of each object, among other parameters. Roughly speaking, a greater Chirp Mass leads to a higher frequency and a larger change in frequency over time. Additionally, if the combined radius is smaller, the peak frequency is higher. Similar to NICER, researchers determine properties of neutron stars using simulations of gravitational-wave signals that are compared with observations (Abbott et al., 2017).

III. METHOD

In order to calculate the probability of an EOS using data, I utilized Bayesian analysis, a statistical method for finding the probability of a statement (e.g., that a hypothesis holds or certain data is observed) given another statement (Kurt, 2019). Bayesian analysis is based on Bayes' theorem, which states that the conditional probability of hypothesis H given data D equals the conditional probability of D given H times the probability of H divided by the probability of D:

$$P(H|D) = \frac{P(D|H)\,P(H)}{P(D)}, \quad (3)$$

which follows from the definition of conditional probability, $P(H|D) = P(H\ and\ D)/P(D)$. Bayes' Theorem provides a rule for updating the prior probability, $P(H)$, of the hypothesis to the posterior probability, $P(H|D)$, to account for the data D.

In the context of this paper, the conditional probability of an EOS given several datasets is equal to the product of the conditional probabilities of each dataset:

$$P(EOS|data) = P(EOS|M_{max}) \times P(EOS|NICER) \times P(EOS|LIGO) \quad (4)$$

since each observation is independent from each other. With Bayes' theorem, the probability of an EOS given data is proportional to the probability of each dataset given an EOS multiplied by the unconditional probability of that EOS. For instance,

$$P(EOS|M_{max}) = P(M_{max}|EOS)\,P(EOS)\,/\,P(M_{max}), \quad (5)$$

With similar relations for $P(EOS|NICER)$ and $P(EOS|LIGO)$, we get:

$$P(EOS|data) \propto P(M_{max}|EOS) \times P(NICER|EOS) \times P(LIGO|EOS) \quad (6)$$

I illustrate my Bayes' theorem methodology in Fig. 5. Because neutron star data is given in mass and radius, I start with many possible EOS candidates (a) and convert them into mass-radius curves (b). Then, in (c), I find two curves (colored yellow) that are most probable

according to dataset 1. Since the dataset consists of discrete points, I construct a probability density function using KDE, available in the SciPy Python library. The basic idea is that more data points in an area represents higher probability. To constrain the mass-radius curves, I calculate the probability of each EOS using Bayesian statistics. This involves determining the probability of each mass-radius point along the curve and summing to obtain the probability of that entire mass-radius curve. Next, in (d), I compute the joint probability using both datasets. The two datasets imply that the one curve (colored red) is more probable. Finally, in (e), I map the mass-radius curves back to their respective EOSs.

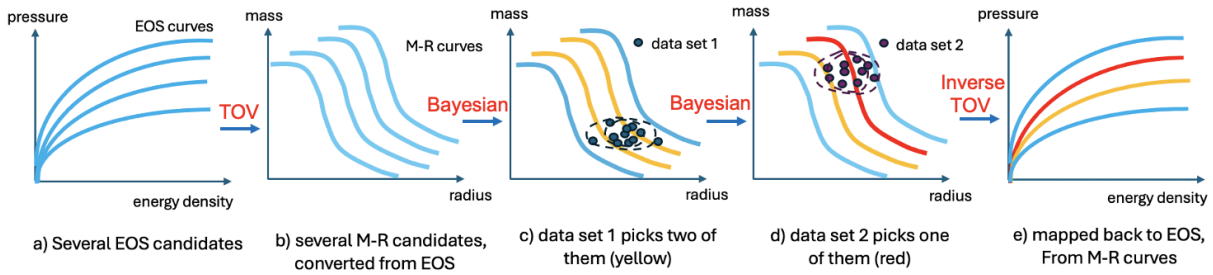

Figure 5: Schematic representation of how I constrain the EOSs using data. a) I start with several, equally-probable EOS candidates, which is indicated by the same blue color. b) Each EOSs is mapped to a mass-radius curve. c) Dataset 1 identifies two mass-radius curves (in yellow) as more probable. d) Dataset 2 further constrains the mass-radius curves by assigning higher probability to the red EOS. e) Finally, the mass-radius curves are mapped back to their respective EOSs along with their probabilities.

IV. PROCEDURE

The procedure of constraining EOSs is based on the methodology in the previous section; the flowchart of Fig. 6 follows the schematic diagram of Fig. 5. After converting EOS to mass-radius curves, I applied five datasets from NICER and LIGO/VIRGO (steps 1-5), and then converted the mass-radius curves with their associated probabilities back into the EOS curves. Afterwards, I analyze the EOSs to find the composition of neutron star cores. All computations were performed by Python programs written by the author.

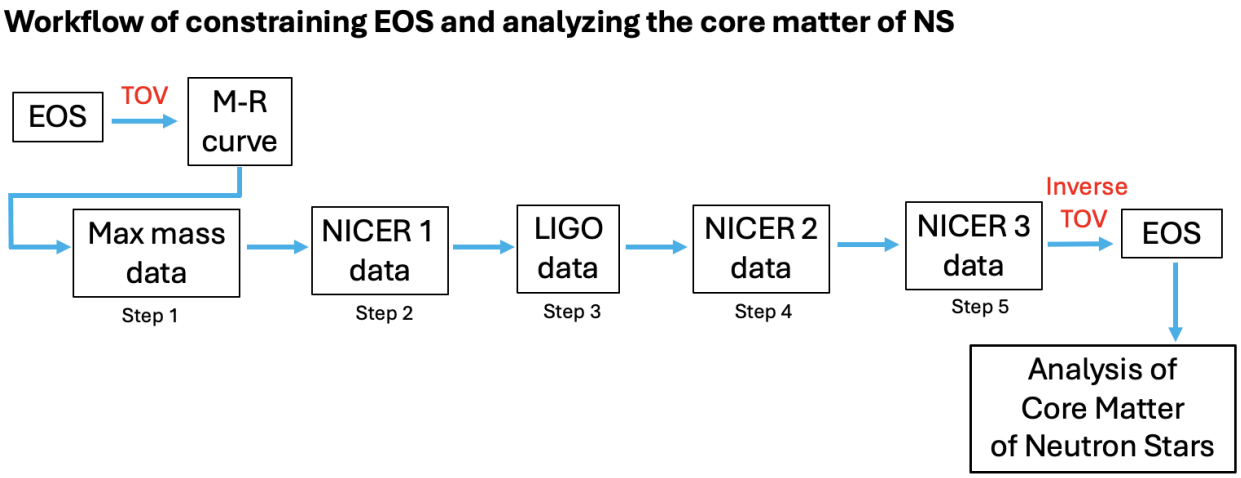

Figure 6: Flowchart of the multistep procedure. From the EOS samples, mass-radius curves are constructed by solving the TOV equations. These curves are then progressively constrained by incorporating the data (step 1-5). Next, the mass-radius curves are mapped back to EOS space. Finally, neutron star cores are analyzed using the probabilities of the EOSs.

To investigate the composition of the core, I separate the EOSs into two categories: those with a first-order phase transition and those without. I use my Python program to identify sections of the EOS where the sound speed is zero for a considerable range, which corresponds to a phase transition. After separating the EOSs, I find the relative probability between no phase transition and a phase transition, which corresponds to nucleonic matter and quark matter, respectively. I sum the probabilities of the EOSs without a phase transition and divide by the sum of the probabilities of the EOSs with a phase transition. Finally, I account for the bias that 11% of the 5000 EOSs have a phase transition.

V. COMPUTATION

I have written three programs for this project. The first is the TOV solver that calculates mass-radius for each EOS. The second is constraining EOS based on the data. And the last is for analyzing the constrained EOS to find the probability of phase transition in the neutron star cores. In this section, I explain these three codes. All codes are written in Python and provided along with the report.

5.1 TOV Solver

The Tolman-Oppenheimer-Volkoff equations for a spherically symmetric body consist of Eqs. 1 and 2, which represent the balance between relativistic gravity and the strong nuclear force. After setting $c = 1$ and simplifying, the TOV equations become

$$dm/dr = 4\,\pi\, r^2\, \epsilon(P)\ ,$$

$$dP/dr = -\ G\,[\epsilon(P) + P]\,\frac{m + 4\,\pi\, r^3\, P}{r\,(r - 2\,G\,m)}\ .$$

The TOV equations form a system of ordinary differential equations (ODEs) to be solved for certain initial conditions:

$$dy/dx = f(x, y),$$
$$y(x_0) = y_0.$$

I wrote a solver that integrates these equations using the forward Euler method. The discretized equations are

$$x_{k+1} = x_k + \Delta x,$$
$$y_{k+1} = y_k + f(x_k, y_k)\,\Delta x.$$

These equations are applied for $k = 0,\ 1,\ 2,\ \ldots$ until a stopping criterion is triggered.

For the TOV equations, y stands for the mass m and pressure P while x stands for the radius r. To model a neutron star, I start at the core of the star ($r = 0$) and integrate until the surface of the star is reached ($r = R$). The pressure at $r = 0$ is the core pressure P_c, whereas the mass is zero at $r = 0$. These values give the initial conditions. Since the core pressure is unknown and different in each neutron star, I choose a range of values for P_c. (See Fig. 3, where various core pressures correspond to their respective points on the mass-radius curve.) In contrast, the

pressure at the surface $r = R$ is zero because it is in equilibrium with the vacuum, whereas m at the surface equals the mass M of the star. The stopping criterion is $P = 0$, and then R is the value of r and M is the value of m.

However, it is important to note that the first step of the integration requires special treatment. The reason is that the right-hand side of Eq. (2) (the equation for pressure) is singular when $r = 0$. I analyzed the singularity and circumvented it in the following way.

While r remains small, $\epsilon(P)$ stays close to the constant $\epsilon_c = \epsilon(P_c)$. Therefore, Eq. (1) implies that

$$m \approx (4\pi r^3/3)\,\epsilon_c.$$

This result is easy to understand: the mass equals the mass-energy density times the volume of a sphere of radius r. After making this substitution, Eq. (2) becomes

$$dP/dr \approx -G(\epsilon_c + P_c)\frac{(4\pi r^3/3)\,\epsilon_c + 4\pi r^3 P_c}{r\left(r - 2G(4\pi r^3/3)\,\epsilon_c\right)}.$$

Since r^3 is much smaller than r, the denominator is approximately r^2, so that

$$dP/dr \approx -4\pi G(\epsilon_c + P_c)(\epsilon_c/3 + P_c)\,r.$$

Hence, for small r, the pressure approximately equals

$$P \approx P_c - 2\pi G(\epsilon_c + P_c)(\epsilon_c/3 + P_c)\,r^2.$$

These approximations replace the first step of the integration. After the first step, the forward Euler method is used.

5.2 Probability Density Function from Discrete Data using Kernel Density Estimator (KDE)

A Kernel Density Estimator (KDE) is a statistical tool to obtain a probability density function, given a data sample. That is, using KDE, we get a smooth function that approximates the underlying probability that could have generated the data themselves. In a sense, it is similar to making a histogram of data and connecting the bars to get a continuous function. To use the KDE, we need to specify the kernel function (K), a smooth function that peaks where the data point is, and the bandwidth. By overlapping the kernel functions with their centers at the data points, we get an estimate of the underlying functions for the data:

$$\widehat{f}(x) \ = \Sigma_{observation} K(\frac{x-observation}{bandwidth})$$

where $\widehat{f}(x)$ is the estimated probability density and the choices for kernel function and bandwidth are problem-dependent.

For the neutron star mass-radius data, I used a 2D KDE with a Gaussian kernel from which I calculated the probability of each mass-radius curve: I picked the fixed number of discrete points along a curve, calculated the probability at each point and then added them up to find the probability of that particular mass-radius (or equivalently, EOS) curve. I repeat this process for the 5000 mass-radius curves. Since I had multiple sets of data, there is a different KDE for the new dataset added in each step, described in Fig. 6.

5.3 Posterior Analysis: Phase Transition Locator

Phase transitions from nucleonic matter to deconfined quark matter are embedded in some of the EOSs I considered. They were randomly generated at different energy density and pressure for random strength (energy required to complete the transition). I wrote a Python script to locate any phase transition which would be manifested as a plateau in the pressure vs. energy

density curves. Specifically, for each EOS, I calculated slopes at grid points and found where they are sufficiently small. One requirement is that the difference in energy density from the start to the end of the phase transition must be at least 50 MeV fm^{-3}. The phase transition must also start within the range of core energy densities, from 150 MeV fm^{-3} to the maximum described by the EOS (Tews, 2024). I performed a further analysis on phase transitions in neutron stars by finding pair correlations among the initiation energy density, max slope, and strength of the phase transition using the corner module in Python.

VI. RESULTS

After generating the neutron star EOSs, converting them into mass-radius curves using the TOV equations, and obtaining mass-radius probability distributions from data, I applied Bayes' theorem to determine the probability of each EOS. As a quantitative measure of how much the mass-radius curves have been constrained, I also calculated the 90th percentile radius interval for a 1.4-solar-mass neutron star.

Step 1: Maximum Mass

We start with the maximum mass data to constrain the mass-radius curves. Each curve predicts a maximum mass, and if that prediction is lower than what has been observed, that particular curve cannot describe massive neutron stars. Therefore, we can exclude such mass-radius curves. In Fig. 7 b), more probable mass-radius curves are dark red while less probable curves are lighter. Since the maximum mass data itself has a probability distribution, the mass-radius curve that predicts the most likely maximum mass has a higher probability than a mass-radius curve with a different maximum mass. The green lines indicate the 90th percentile range of the maximum mass, which I call the upper and lower bounds.

Using these constrained mass-radius curves, we plot the probability distribution for the radius of a 1.4-solar-mass neutron star (Fig. 8b). The 90th percentile range of the predicted radius is $11.52^{+1.31}_{-1.58}$ km.

After constraining the mass-radius curves, I found that the odds of a first-order phase transition (FOPT) is about 1/18, indicating that most EOSs with FOPT are discarded.

Steps 2, 3, 4, and 5: NICER 1, LIGO, NICER 2, and NICER 3

Having selected the EOSs that satisfy the maximum mass constraint, I apply the NICER 1 (PSR J0030+0451) data. The green contours (at 1 and 2 standard deviations) in Fig. 7c represents the high probability region according to NICER 1. Hence, the EOS curves that go through the green contours are evaluated to have high probability. In Fig. 8c, I plot the probability distribution of the radius of a neutron star at 1.4 solar mass.

I progressively use the LIGO (GW170817) and the other NICER data in addition to the previous data. The LIGO data comes from observing two merging neutron stars. The green contours in Fig. 7d represent the more massive neutron star, and the blue contours represent the less massive neutron star. The NICER 2 (PSR J0437-4715) data, shown in Fig. 7e, has not been used in previous work. Lastly, I use the NICER 3 (PSR J0740+6620) data. This pulsar is heavy, at about 2 solar masses, and its NICER data has also not been used previously. As seen in Fig. 7f, I now have a much smaller number of EOS that are probable, according to the data. I note the population of the allowed EOSs is reduced as I constrain them with more data. In Fig. 8f, I plot the final radius probability distribution of a 1.4-solar-mass neutron star. The final distribution has a much narrower peak at about 11.5 km, compared with Fig. 8a, for which the radius is unconstrained.

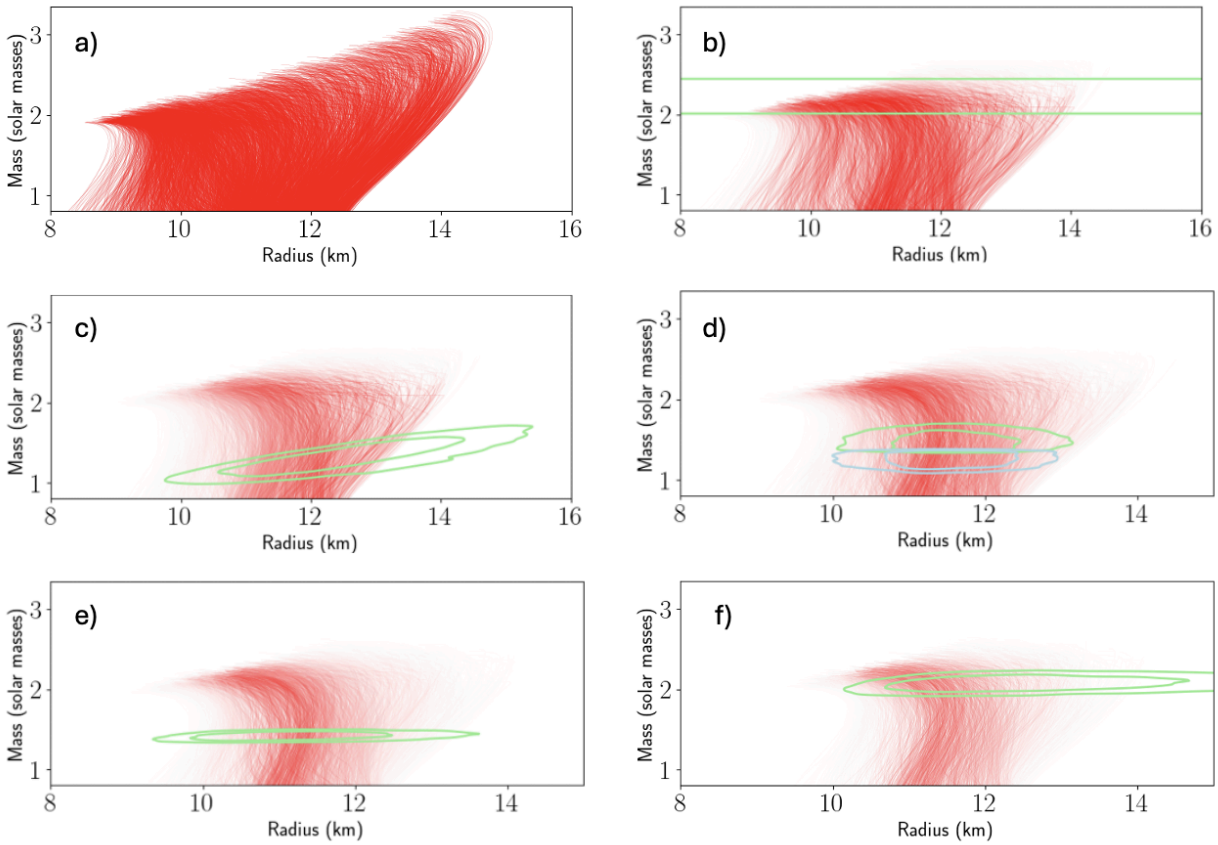

Figure 7: Constraining the mass-radius curves using the data. a) The initial set of 5000 EOSs with no constraints. b) Mass-radius curves constrained by the maximum mass data from PSR J0740+6620, PSR J0348+4032, PSR J0614-2230, and GW170817. The green lines represent the upper and lower mass bounds. c) Mass-radius curves further constrained by the NICER data of PSR J0030+0451. The green contours are at the 95% and 68% confidence level. d) Further constraints by LIGO (GW170817) data. Green contours are at the 95% and 68% confidence level for the more massive neutron star, with the blue contours representing the less massive neutron star. e) Further constraints on mass-radius curves by PSR J0437-4715 data. f) Further constraint by PSR J0740+6620.

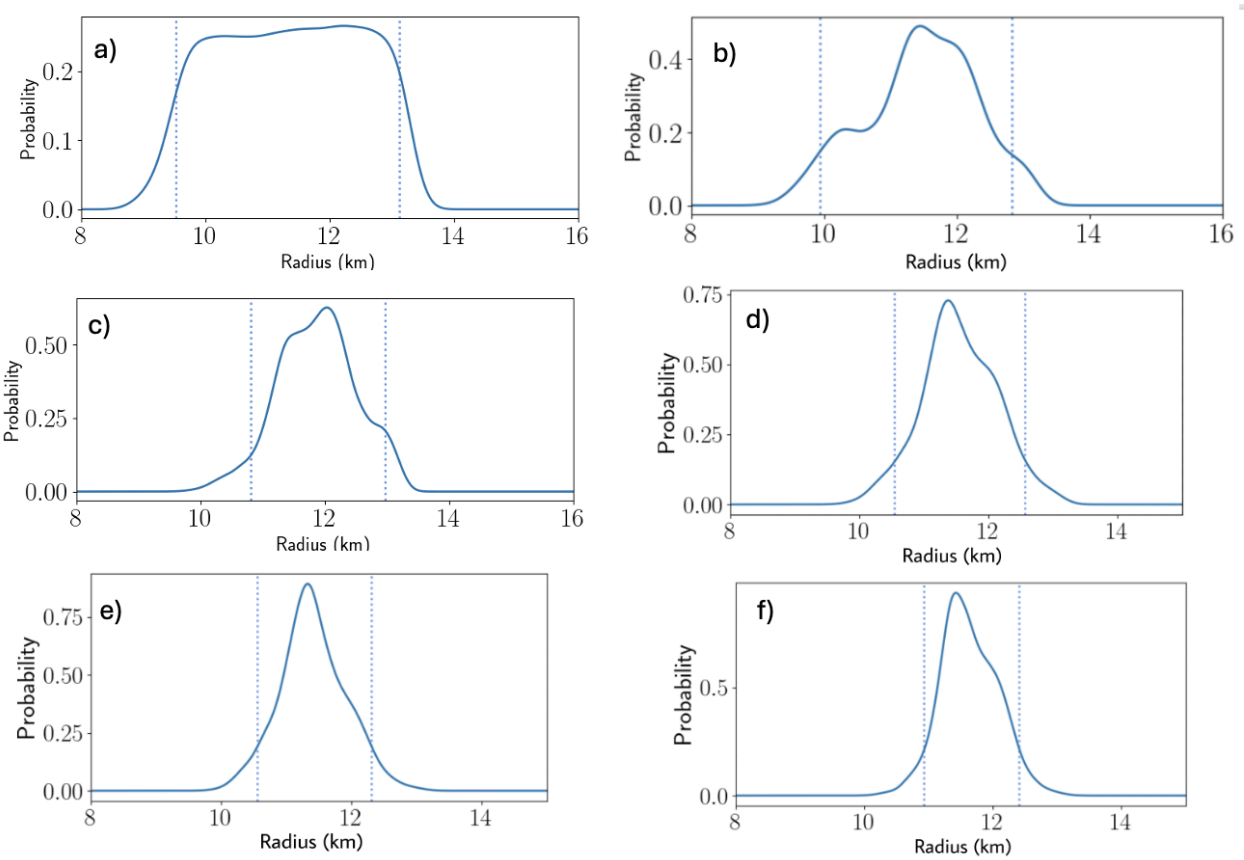

Figure 8: Probability distribution of radius for a neutron star with 1.4 solar masses. a) Before constraining. b) Constrained by the maximum mass data, c) the NICER 1 data, d) the LIGO data, e) the NICER 2 data, and f) the NICER 3 data.

In Table 2, I summarize the predictions of the radius of a 1.4-solar-mass neutron star from each step. The uncertainty is reduced in each step.

	Initial set	**Max mass**	**NICER 1**	**LIGO**	**NICER 2**	**NICER 3**
The radius of a 1.4 solar mass NS (90% confidence, km)	$11.37^{+1.75}_{-1.85}$	$11.52^{+1.31}_{-1.58}$	$11.88^{+1.09}_{-1.09}$	$11.53^{+1.04}_{-0.98}$	$11.38^{+0.92}_{-0.83}$	$11.60^{+0.81}_{-0.67}$

Table 2. The radius prediction of a neutron star with 1.4 solar mass. The intervals are the 90th percentile intervals and correspond to the vertical lines in Figs. 8a, 8b, 8c, 8d, 8e, and 8f.

Now that we have obtained the allowed set of EOSs, we can compare them with theory-based models. In Fig. 9, we plotted the predictions of mass and radius by the various models (Lattimer and Prakash, 2001, Gandolfi et al., 2019) overlapped onto Fig. 7 (f). Each of these models assume a certain composition of the core: the orange curves predict only quark matter (Prakash, M. *et al.,* 1995), the blue ones for nucleonic (Akmal and Pandharipande, 1997, Müller and Serot, 1996, Wiringa, R. B, 1988), and the green curves for mixtures of nucleonic and exotic matter (Prakash, M. *et al*, 1995, Glendenning *et al.,* 1991, Glendenning *et al.,* 1999). Clearly, many of the models don't agree with the current data-based predictions. Those that fall in the range of the allowed EOSs are for the nucleonic matter, hence it implies that the phase transition to quark matter or other exotic matter is unlikely.

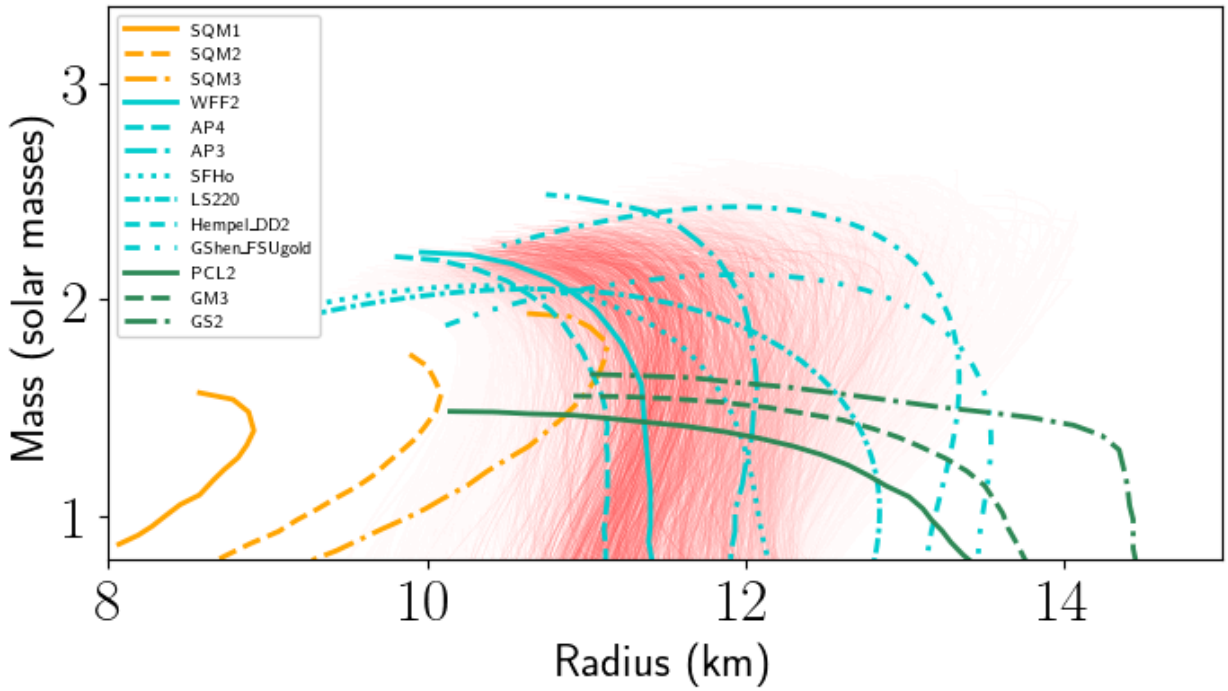

Figure 9: Comparison between the theory-based models and the data-based predictions of mass-radius curves. The orange curves are for quark matter only, the blue ones are for nucleonic matter, and the green curves for nucleonic, quark, and hyperon mixtures.

Having found the probabilities of the EOSs, I mapped the mass-radius curves back to EOS space. In Fig. 10, I show the spread of all EOSs I considered in dark blue and the allowed EOSs in light blue in pressure vs. energy density space. Up to the energy density at about 250

MeV/fm^3, all EOSs obey Chiral Effective Field Theory and there is little uncertainty. Beyond that point, I find the pressure increase was needed while some of the highest pressures were not feasible.

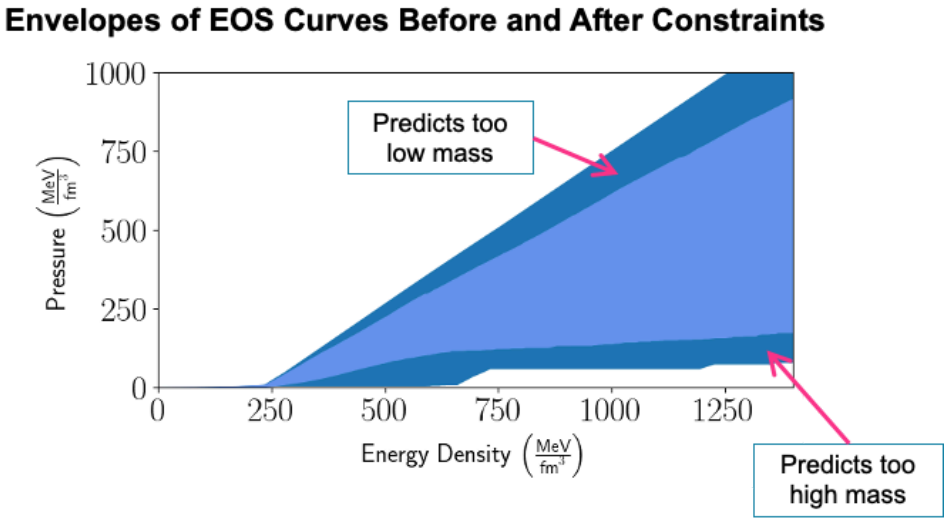

Figure 10: Envelopes of probable EOSs before and after constraints, in pressure vs. energy density space. The dark blue region represents the full set of EOSs considered, with every EOS lying within it. The light blue region shows the extent to which the EOSs were constrained, representing the 90th percentile range of EOSs after the constraints by the data. I emphasize that this plot shows the envelope of the EOS curves and does not imply that an arbitrary EOS going through the shaded region is allowed or even considered.

After constraining the mass-radius curves, finding the 90th percentile radius intervals of a 1.4 solar mass neutron star, and mapping the probabilities back to the corresponding EOSs, I separated the EOSs with and without phase transitions. In Table 3, I summarized the relative probabilities of first-order phase transitions (FOPT) to no phase transition calculated in each step of constraining EOSs. To find the relative probability, I calculate the likelihood of a phase transition by summing the probabilities of the EOSs with a phase transition. Then, I divide by the likelihood of no phase transition, which is calculated similarly, and multiply by a factor that accounts for the unequal number of EOSs with and without a PT.

Most EOSs that have a PT were eliminated in the first step since those EOSs have a maximum possible mass above 2 solar masses. The EOSs without PTs are preferred by the remaining data sets as well. After the final step of constraining EOSs, the odds of a FOPT to no

PT is about 1 to 21. This is consistent with the findings from Fig. 9 that the EOSs with quark matter or other exotic matters do not predict the data as well as those with only nucleons.

	Initial set	Max mass	NICER 1	LIGO	NICER 2	NICER 3
Odds of FOPT to no PT	1:1	1:16.87	1:19.07	1:19.16	1:19.68	1:20.78

Table 3: Odds of a first-order phase transition to no phase transition in each step of constraintment.

In Figure 11, I plot the constrained EOSs in the two groups. Since I am investigating phase transitions in the cores of neutron stars, I truncated the EOS curves at their respective maximum central pressure, which varies from EOS to EOS.

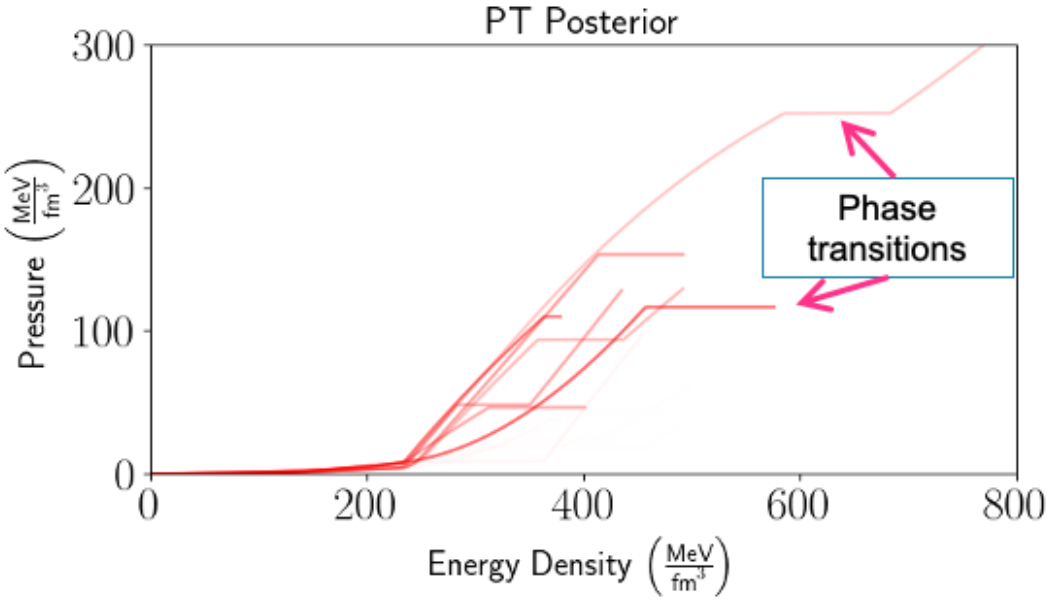

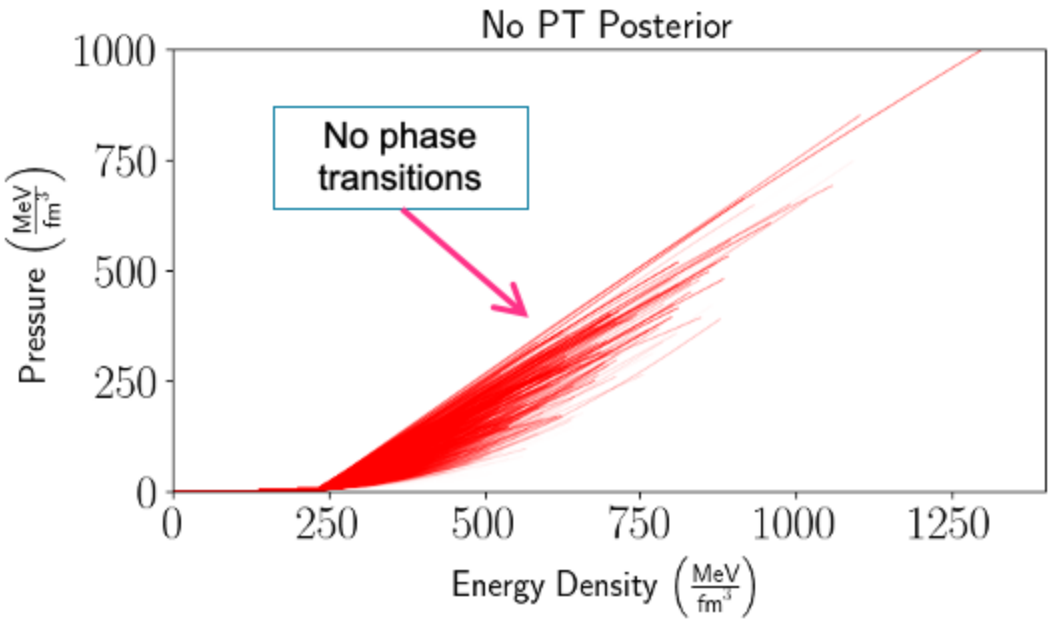

Figure 11: Likely EOSs in two groups. a) The EOSs that predict first-order phase transitions cc(PT) at the core; b) the EOSs that predict no first-order phase transitions in neutron stars. In both plots, curves are truncated at the maximum possible central pressure.

In Fig. 11 (a), I note that the phase transition starts and completes at different energy densities so I performed a statistical analysis on the parameters that characterize the phase transition as shown in Fig. 11 where epsilon is the energy density and sound speed squared (c^2) is the slope of pressure-energy density curve. We observe that the phase transition starts at an energy density (epsilon start) of about 276 MeV/fm^3 and that the change in energy density over the phase transition (epsilon difference) is about 218 MeV/fm^3. While the initiation energy density is not strongly correlated to the energy density jump, the latter and the sound speed after the phase transition indicate a positive correlation, meaning that the more energy needed for a phase transition, the larger the sound speed after the PT is.

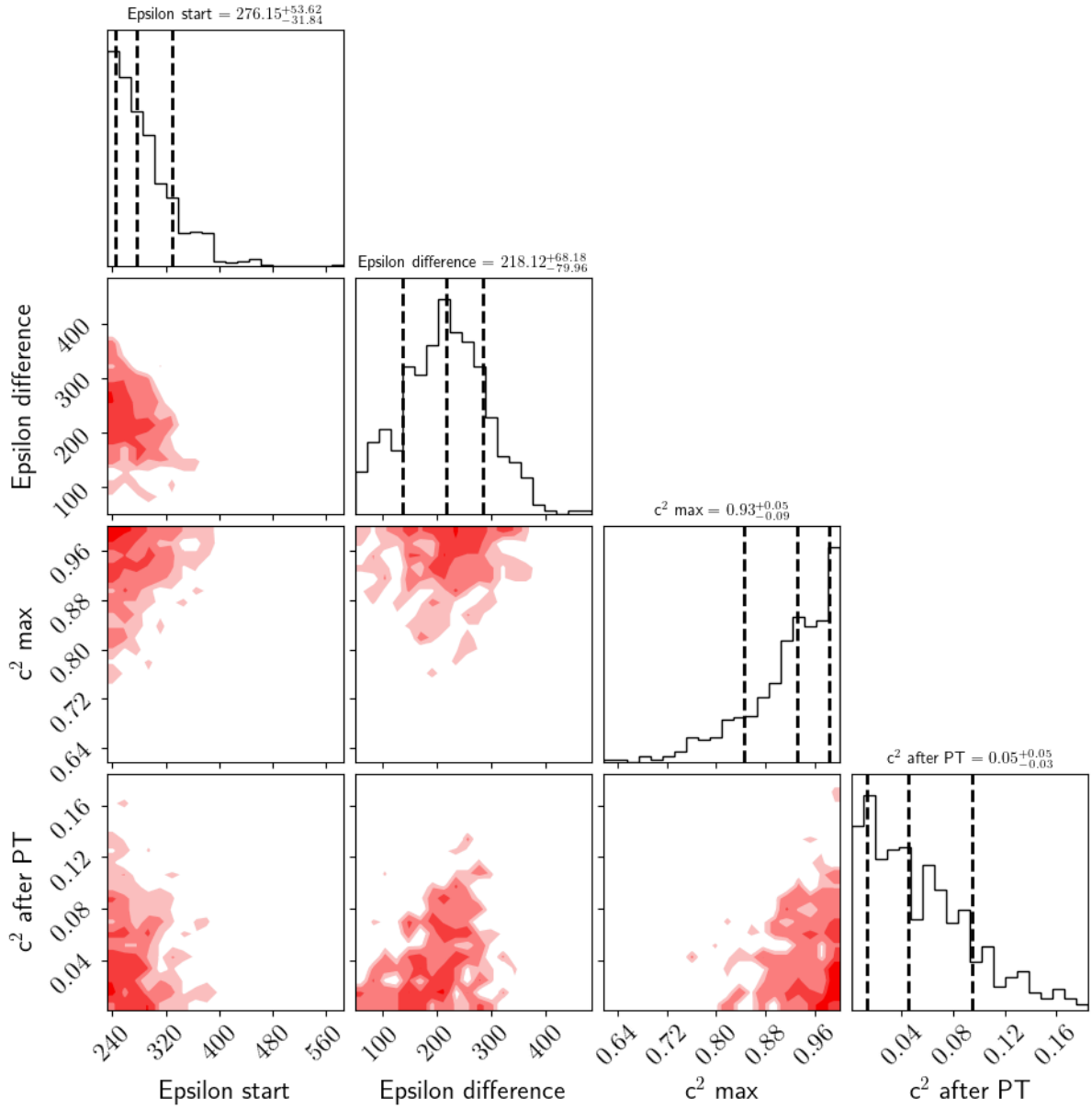

Figure 12: Pair plots for the phase transition parameters. For each parameter, we show the mean value and one standard deviation. "Epsilon start" is where the phase transition initiates in energy density and "Epsilon difference" is the jump in energy density occurring during the phase transition. "c^2 max" is the maximum sound speed squared for each EOS in the entire range of energy density and "c^2 after PT" is the value of the sound speed right after the phase transition.

VII. CONCLUSIONS

I successfully developed software that solves the TOV equations and analyzes observations of neutron stars in a Bayesian statistical framework to determine the probability of a given mass-radius curve. Among the five data sets used, the first three had been previously analyzed in a similar manner (Dietrich *et al*., 2020**)** and I verified that my results were consistent with theirs. I incorporated two new data sets, further constraining the neutron star EOS. In addition, I examined the allowed EOSs to investigate the possibility of a phase transition at the core. There are two main results in this paper.

1) First is a stronger constraint of the mass-radius curves using the new data from NICER (PSR J0437-4715, PSR J0740+6620). My result is that the 90th percentile interval for the radius of a 1.4 solar mass neutron star is $11.60^{+0.81}_{-0.67}$. After determining the mass-radius curves that are most probable given the data, I mapped those curves back to the pressure-energy density space to find the constrained EOS models of neutron star matter (Fig. 10). The dark blue region represents the range of EOSs considered before applying data constraints, while the light blue region shows the EOSs allowed by the data. My analysis eliminated many EOS curves. This can be also seen in Fig. 9 where the mass-radius prediction of the various theory-based models are plotted along with the constrained curves.
2) Second, I categorized the EOSs based on whether they had a first-order phase transition (FOPT) or not, which predicts deconfined quark matter or nucleonic matter, respectively, in the core. My data-oriented analysis shows that a FOPT is not likely in the core of the neutron stars. Which is consistent with the findings that EOSs that contain any exotic matter are unlikely, as seen in Fig 9. This contrasts with Annala et al. (2020), which claims that a phase transition is necessary. One thing to note is that I considered only first-order phase transitions since mixed phase transitions are not easily or definitively found from the EOS.

APPENDICES

Bimodal Reanalysis of NICER 1 (PSR J0030+0451)

Recently, the NICER team released the results of the reanalysis of PSR J0030+0451 using an updated calibration framework and simulation capabilities (Vinciguerra *et al.* 2024). The reanalysis contains two modes, meaning there are two likely sets of mass-radius values. These modes were obtained by using two different models for the hot spots (locations, morphology, etc.) on the neutron stars in their simulations. I use the methodology developed in this work to find which mode is more likely according to the other neutron star data. That is, I use the Max Mass, LIGO, NICER 2, and NICER 3 data to find the probabilities of the mass-radius curves as in the method and procedure sections. Then by comparing the constrained mass-radius curves to the reanalyzed mass-radius data of NICER 1, I found what mass and radius are probable for PSR J0030+0451. In Fig. 11, there are two sets of contours that correspond to the different modes. The first mode (blue contours) generally predicts lower mass and radius compared to the second mode (green contours). The constrained mass-radius curves fit the first mode of the analysis so I conclude that the first mode is more probable and a better model of neutron stars.

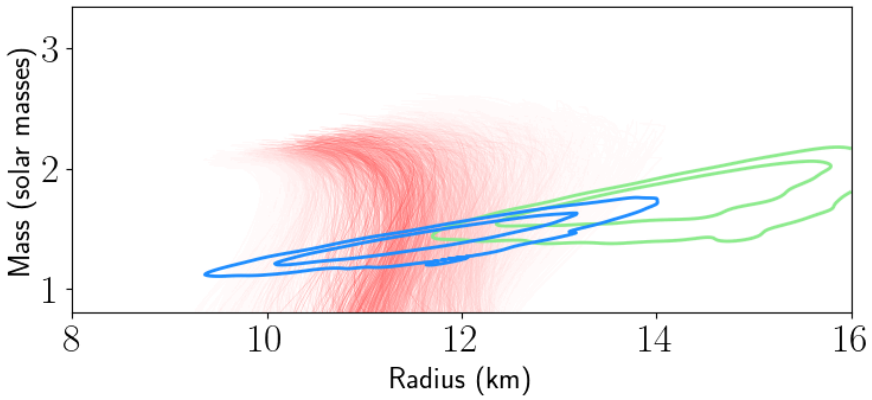

Fig. 11. Bimodal analysis of PSR J0030+0451 with constrained mass-radius curves. Mode 1 (blue contours) is found to be more probable since it fits the mass-radius curves better.

ACKNOWLEDGEMENTS

I thank Drs. Ingo Tews and Rahul Somasundaram for their mentorship on this project, both at Los Alamos National Laboratory. I also thank my parents, Dr. JeeYeon Plohr and Dr. Bradley Plohr, for guidance and support.

REFERENCES

Abbott *et al*. GW170817: Observation of gravitational waves from a binary neutron star inspiral, *Phys. Rev. Lett.* 2017, 119.

Akmal, A., and Pandharipande, V.R Spin-isospin structure and pion condensation in nucleon matter, Phys. Rev. C, 1997, 56, 226.

Annala et al. Evidence for quark-matter cores in massive neutron stars, *Nat. Phys*. 2020, 16.

Antoniadis, J. *et al.* A massive pulsar in a compact relativistic binary, *Science* 2013, 340.

Arzoumanian, Z. *et al.* The NANOGrav 11-year dataset: High-precision timing of 45 millisecond pulsars, *Astrophys. J. Suppl.* 2018, 235.

Benhar, O. *et al.* (eds.) Nuclear Theory in the Age of Multimessenger Astronomy. CRC Press, 2024.

Camenzind, M. Compact Objects in Astrophysics: White Dwarfs, Neutron Stars and Black Holes, Springer, 2007.

Capano, C. *et al*. Stringent constraints on neutron-star radii from multimessenger observations and nuclear theory, *Nature Astr*. 2020, 4.

Caplan, M.; Horowitz, C. Astromaterial Science and Nuclear Pasta, *Rev. Mod. Phys.* 89, 041002, 2017.

Choudhury, D. *et al.* A NICER View of the nearest and brightest millisecond pulsar: PSR J0437-4715, arXiv: 2407.06789, 2024.

Cowan, J. *et al.* Origin of the heaviest elements: The rapid neutron-capture process, *Rev. Mod. Phys.* 2021, 93.

Cromartie, H. T. *et al*. Relativistic Shapiro delay measurements of an extremely massive millisecond pulsar, *Nature Astron*. 019, 4.

Dietrich, T. *et a*l. Multimessenger constraints on the neutron-star equation of state and the Hubble constant, *Science* 2020, 370.

Epelbaum, E., *et al.* Modern Theory of Nuclear Forces, *Rev. Mod. Phys.* 2008, 81.

Gandolfi, S. *et al.* From the microscopic to the macroscopic world: from nucleons to neutron stars, *J. Phys. G: Nucl. Part. Phys.* 2019, 46.

Glendenning, N. K., & Moszkowski, S. A. Reconciliation of neutron star masses and binding of the Λ in hypernuclei, Phys. Rev. Lett., 1991, 67, 2414.

Glendenning, N. K., & Scha†ner-Bielich, J. First order kaon condensate, Phys. Rev. C., 1999, 60, 025803

Kobyakov, D. Application of superconducting-superfluid magnetohydrodynamics to nuclear "pasta" in neutron stars, *Phys. Rev. C*, 045803, 2023, 98.

Kurt, W. Bayesian statistics the fun way. No Starch Press, Inc., 2019.

Lattimer, J. M. and Prakash, M. Neutron Star Structure and the Equation of State, *Astrophys. J.* 2001, 550:426.

Miller, M. C. *et al.* PSR J0030+0451 Mass and radius from NICER data and implications for the properties of neutron star matter, *Astrophys. J. Lett*. 2019, 887.

Miller, M. C. *et al.* The Radius of PSR J0740+6620 from NICER and XMM-Newton Data, *Astrophys. J. Lett.* 2021, 918.

Müller, H. and Serot, B. Relativistic mean field theory and high density nuclear equation of state, Nuclear Physics A, 1996, 606.

Oppenheimer, J. R.; Volkoff, G. M. On massive neutron cores, *Phys. Rev*. 1939, 55.

Prakash, M., Cooke, J. R., & Lattimer, J. M. Quark-hadron phase transition in protoneutron star, Phys. Rev., D52, 1995, 661.

Raaijmakers, G. *et al.* A NICER view of PSR J0030+0451: Implications for the dense matter equation of state, *Astrophys. J. Lett.* 2019, 887.

Rezzolla, L. *et al.* Using gravitational-wave observations and quasi-universal relations to constrain the maximum mass of neutron stars, *Astrophys. J.* 2018, 852.

Riley, T. E. *et al.* A NICER View of the Massive Pulsar PSR J0740+6620 Informed by Radio Timing and XMM-Newton Spectroscopy, *Astrophys. J. Lett.* 2021, 918.

Somasundaram, R.; Tews, I.; Margueron, J. Investigating signatures of phase transitions in neutron-star cores, *Phys. Rev. C*, 2023, 107, 025801.

Tews, I. Private communication, 2024.

Tews, I. *et al*. Constraining the speed of sound inside neutron stars with chiral effective field theory interactions and observations, *Astrophys. J.* 2018, 860:149.

Tolman, R. C. Static Solutions of Einstein's Field Equations for Spheres of Fluid. *Phys. Rev.*1939, 55, 364.

Vinciguerra, S. *et al.* An updated mass-radius analysis of the 2017-2018 NICER dataset of PSR J0030+0451, *Astrophys. J.* 2024, 961.

Watts, A. *et al.* Measuring the neutron star equation of state using X-ray timing, *Rev. Mod. Phys.* 2016, 88(2):021001.

Wiringa, R. B., Fiks, V., & Fabrocine, A., Equation of state for dense Nucleon matter, Phys. Rev. C, 1988, 38, 1010.

Zhang, Z-W and Pethick, C. J. Proton superconductivity in pasta phases in neutron star crusts, *Phys. Rev. C* 2021, 103.